Transverse manipulation of particles using Bessel beam of tunable size generated by cross-phase modulation

Xiang-Lai Qiao(乔响来)[1], Xue-Mei Cheng(程雪梅)[1,†], Qian Zhang(张倩)[2,‡], Wen-Ding Zhang(张文定)[1], Zhao-Yu Ren(任兆玉)[1], and Jin-Tao Bai(白晋涛)[1]

[1] *State Key Laboratory Incubation Base of Photoelectric Technology and Functional Materials, National Photoelectric Technology, and Functional Materials and Application of Science and Technology International Cooperation Center, Institute of Photonics & Photon-Technology, Northwest University, Xi'an* 710069, *China*

[2] *China School of Electronic Engineering, Xi'an University of Posts & Telecommunications, Xi'an* 710121, *China*

(Received 15 June 2022; revised manuscript received 2 August 2022; accepted manuscript online 12 August 2022)

We report on a method to achieve multiple microscopic particles being trapped and manipulated transversely by using a size-tunable Bessel beam generated by cross-phase modulation (XPM) based on the thermal nonlinear optical effect. The results demonstrate that multiple polystyrene particles can be stably trapped simultaneously, and the number of the trapped particles can be controlled by varying the trapping beam power. In addition, the trapped particles can be manipulated laterally with micron-level precision by changing the size of J_0 Bessel beam. This work provides a simple but efficient way to trap and manipulate multiple particles simultaneously, which would have potential applications in many fields such as cell sorting and transportation.

Keywords: optical manipulation, optical trapping, J_0 Bessel beam, cross-phase modulation

PACS: 87.80.Cc, 42.62.–b, 42.65.–k **DOI:** 10.1088/1674-1056/ac8925

1. Introduction

Optical tweezers is an optical method in which a highly focused laser beam is employed to trap and manipulate the nano- and micro-sized objects.[1] Since proposition and realization in the 1980s by Ashkin *et al.*,[2] optical tweezers has been applied to numerous areas, such as bio-components identification,[3,4] *in-situ* single particle and graphene analysis[5,6] and light–matter interaction.[7] Laser beam with a Gaussian intensity distribution is commonly used in conventional optical tweezers. However, it is difficult to trap multiple particles simultaneously by using Gaussian beams, because the optical traps are limited within a few micrometers around the focal point resulting from the beam distortion by the particle and high divergence after tight-focusing.[8,9]

The solution to improving the trapping efficiency is to create multiple traps in one setup. So far, there has been several methods reported to generate multiple traps, such as time-shared optical tweezers,[10,11] holographic optical tweezers,[12,13] and interferometric optical tweezers.[14,15] In time-shared optical tweezers, a single Gaussian laser beam is scanned across a region and therefore multiple particles within this region can be trapped one by one. In holographic optical tweezers, multiple optical traps are obtained by focusing multiple sub-beams generated from one incident laser beam with optical diffraction components or spatial light modulators. As for interferometric optical tweezers, multiple beams are interfered to achieve multiple traps with high spatial resolution.

Bessel beams are radiations of which the amplitudes can be described by Bessel functions.[16] The typical zeroth-order (J_0) Bessel beam consists of a bright central spot surrounded by a series of bright rings. Bessel beams have remarkable non-diffraction properties, and hence the beam size and intensity remain constant during propagation. In addition, Bessel beams can reestablish their transverse intensity profile after encountering an obstacle.[17] The excellent propagation characteristics and unique intensity profile of Bessel beam offer an extended working distance and multiple traps for optical trapping and manipulation. Arlt *et al.* have demonstrated that the trapping efficiency of Bessel optical tweezers is 10 times higher than that of conventional Gaussian optical tweezers.[18] Garcés-Chávez *et al*. achieved multiple particles to be trapped in different axial layers and successfully guided the particles to move along the axial coordinate (up to $\sim$ 3 mm) by the diffraction less nature of the Bessel beam.[19] Compared with the study of manipulation along the beam propagating direction, the research of transverse manipulation is still limited. Milne *et al*.[20] demonstrated the motion of silica microspheres of different sizes in a fixed periodic light field provided by a Bessel beam. There are also many experiments on orbital rotation of the particles around the beam axis, mainly by transferring the angular momentum of the laser beam to the particles. For example, Volke-Sepúlveda *et al*. achieved the rotation of low-refractive-index particles around the beam axis by using a helical high-order Bessel beam.[21] Garcés-Chávez *et al.* real-

†Corresponding author. E-mail: xmcheng@nwu.edu.cn
‡Corresponding author. E-mail: qianzhang_03@163.com

© 2023 Chinese Physical Society and IOP Publishing Ltd

ized the rotation of high and low refractive index particles simultaneously around the beam axis through Bessel beam.[22] However, transitional movement in the transverse plane with a controlled manner has rarely been realized.

The positions and sizes of the trapped particles in the transverse plane are dependent on the beam profile (spatial intensity distribution) of the Bessel beam. And therefore, the Bessel beam with tunable size is useful in manipulating the particles and increasing the robusticity in trapping particles of various sizes. However, the intensity distribution is commonly fixed for a specific experimental setup (optical device).[23,24] For example, the device that is most commonly used to generate Bessel beam is axicon lens. As the cone angle of an axicon lens is inherently fixed, the size of the output Bessel beam is always fixed. Spatial light modulators (SLMs) can be used to generate Bessel beams of variable parameters. But the damage thresholds of the SLMs are relatively low, thus limiting the intensity of the generated Bessel beams. Previously, our group proposed and realized a Bessel beam generation method through using cross-phase modulation (XPM). Based on thermo-optical nonlinear effect, ethanol medium works as a tunable spatial light modulator under the irradiation of an intense pump beam. The probe beam can be converted into a Bessel beam with tunable size by adjusting the pump power.[25] It has been demonstrated that the Bessel beam generated with this method possesses high flexibility and high damage threshold.

In this work, we further use the Bessel beam of tunable size generated by XPM to trap and manipulate the particles transversely. Multiple particles can be trapped and manipulated laterally with micron-level precision by changing the size of Bessel beam. This work provides a simple and useful tool for trapping and manipulating mulitple particles, which is of significance for the *in-situ* study of multiple particles in the liquid and for the sorting and transportation of cells.

2. Method

Figure 1 shows the scheme of the experimental setup used in this work. The laser source is a 780-nm continuance-wave laser (UniQuanta, ECL801-780). A half wave plate (HWP) can be used to change the polarization direction of linear polarization beam. And a polarization beam splitter (PBS) can split the input beam into two beams of orthogonal polarizations. Therefore, the combination of an HWP and a PBS can be used to split the input beam into two beams with adjustable power ratio by rotating the HWP. As shown in Fig. 1, HWP 1 and PBS 1 are used to split the laser output into two beams: the reflection from the PBS 1 serves as the pump beam, and the transmission from the PBS1 is used as the probe beam. The pump beam is focused into the cuvette with ethanol solution by a lens with the focal length of $f = 500$ mm. The HWP 2 and PBS 2 are used to control the power of the pump beam in the interaction region. The probe beam is guided into the same cuvette counter, propagating with respect to the pump beam without focusing. The HWP 3 and PBS 3 are used to control the power of the probe beam in the interaction region. The probe beam from the ethanol solution can be converted into a hollow beam due to XPM.[26] The hollow beam is then collimated by a telescope system (lens 2 and lens 3), and then reflected by the dichroic mirror. The hollow beam is further focused by an objective lens (objective 1, 40×, NA = 0.45) and a J_0 Bessel beam can be obtained for trapping and manipulating the particles in the focusing range. An LED light in a wavelength range from 440 nm to 670 nm is used as illumination. The image-acquisition system is used to receive the images of the trapped particles, which includes an objective lens (objective 2, 80×, NA = 0.8) and a CMOS camera (Thorlabs DCC1240M, 1280 × 1024, pixel size: 1.4 μm). Once particle is observed to be captured, we carefully adjust the axial position of the imaging objective (objective 2 in Fig. 1) until a clear image particle is seen.

The particles used for experiments are two types of polystyrene particles (PSs) with an average diameter of ∼ 3 μm and ∼ 10 μm respectively (unibead polystyrene, baseline). Various concentrations of PS suspension are prepared by adding deionized water. The sample suspension (∼ 40 μL each time) is sandwiched between a glass container and a cover glass (0.16 mm in thickness), which can reduce the influence of the limited working distance of the objective lens and the disturbance from airflow. The sample cell is placed on a three-dimensional transitional platform.

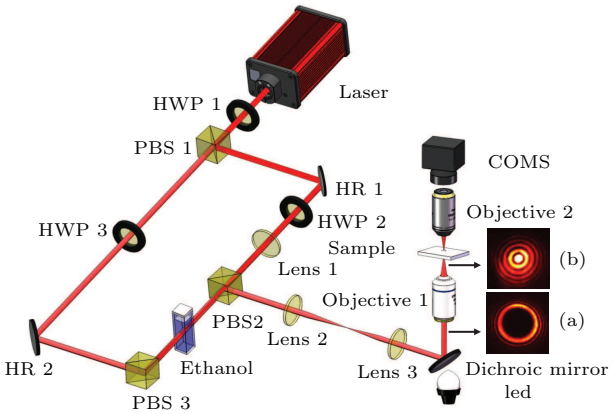


Fig. 1. Schematic diagram of experimental setup. HWP: half-wave plate; HR: highly reflective mirror; PBS: polarization beam splitter; lens 1: $f =$ 500 mm; lens 2: $f = 200$ mm; lens 3: $f = 50$ mm.

In theory, when a focused laser beam illuminates on the micro-sized particles, the light is refracted and reflected by the particles, which would result in the momentum transfer from laser to particles. And then, the gradient force and the scattering force are generated on the particles.[27] In general, for larger spherical objects ($R_0 \gg \lambda$), the optical force and potential energy distribution are related to particle size or geometry,

and the force can be calculated by a ray-tracing method based on Mie scattering theory.[28,29] In this wok, the particles diameter (3 μm) is much larger than the wavelength of the light (780 nm), so the ray tracing method can accurately obtain the size of the trapping force generated by the particles moving in the light field and is widely used to calculate the trapping force on the lateral plane of the particles.[21,22] With the geometrical optics approximation and the same approach used by Gussgard *et al.*,[30] the total force $\boldsymbol{F}$ acting on a transparent spherical particle can be expressed as

$$\boldsymbol{F}=\frac{1}{v_{\mathrm{m}}}\int_{s_1} I\cos\alpha_{\mathrm{i}}\left[\hat{\boldsymbol{u}}_{\mathrm{i}}-R\hat{\boldsymbol{u}}_{\mathrm{r}}-T^2\sum_{k=1}^{N}R^{k-1}\hat{\boldsymbol{u}}_{tk}\right]\mathrm{d}A, \quad (1)$$

where v_{m} is the speed of light in the medium surrounding the particle, s_1 is part of the sphere's surface illuminated by the incident field, I is the intensity distribution of the incident field, α_{i} is the incidence angle with the normal at the incidence point, $\hat{\boldsymbol{u}}_{\mathrm{i}}$ and $\hat{\boldsymbol{u}}_{\mathrm{r}}$ correspond to the incident ray and reflected ray, respectively, $\hat{\boldsymbol{u}}_{tk}$ is the ray transmitted out of the sphere after k internal reflections, N is the total number of internal reflections of the incident rays inside the sphere, and R and T are the reflectance coefficient and transmittance coefficient, respectively.

In order to better describe the optical force exerted on the spherical particle, we employed two coordinate systems, $S(x,y,z)$ and $S'(x',y',z')$. As shown in Fig. 2, the origin of S system is the center of J_0 Bessel beam, and the spherical particle with radius R_0 is located at the $C(r_0,z_0)$ in the coordinate system S. And the center of the spherical particle is taken as the origin of the coordinate system $S'(x',y',z')$ with z' parallel to z. And therefore, the coordinates of a random point on the particle P in the S system is obtained as follows:[22]

$$r=[r_0^2+R_0^2\sin^2\theta+2r_0R_0\sin\theta\cos\phi]^{1/2}, \quad (2)$$

$$z=z_0+R_0\cos\theta, \quad (3)$$

where θ and ϕ are the polar angle and the azimuthal angle in the coordinate system respectively, *i.e.*, the angle from CP to z' and from CP to x', respectively.

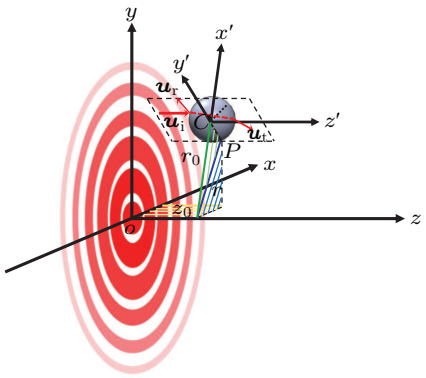


Fig. 2. Geometrical parameters of general ray tracing model for a spherical particle irradiated by Bessel beam propagating along z direction.

The intensity distribution of J_0 Bessel beam is azimuthally symmetric, and therefore only the energy flux propagating along the z direction is considered. After some vectorial calculations based on the geometrical relation from Fig. 2, the unit vectors of the incident ray $\hat{\boldsymbol{u}}_{\mathrm{i}}$, reflected ray $\hat{\boldsymbol{u}}_{\mathrm{r}}$ and transmitted ray $\hat{\boldsymbol{u}}_{tk}$ can be obtained, and the radial optical force F_ρ and axial force F_z acting on the spherical particle of radius R_0 can be expressed as[20,25]

$$\begin{aligned}F_\rho(r,z) &= \frac{R_0^2}{2v_{\mathrm{m}}}\int_0^{\pi/2}\int_0^{2\pi}\Bigg[R\sin 2\theta\\ &\quad -T^2\left(\frac{\sin 2(\theta-\theta_{\mathrm{t}})+R\sin 2\theta)}{1+R^2+2R\cos 2\theta_{\mathrm{t}}}\right)\Bigg]\\ &\quad \times I(r_0,z_0)\sin 2\theta\cos\phi\,\mathrm{d}\phi\,\mathrm{d}\theta, \quad (4)\\ F(z) &= \frac{R_0^2}{2v_{\mathrm{m}}}\int_0^{\pi/2}\int_0^{2\pi}\Bigg[\cos(\theta_{\mathrm{i}}-\theta)+R\cos(\theta_{\mathrm{i}}+\theta)\\ &\quad -T^2\left(\frac{\cos(\theta_{\mathrm{i}}+\theta-2\theta_{\mathrm{t}})+R\cos(\theta_{\mathrm{i}}+\theta)}{1+R^2+2R\cos 2\theta_{\mathrm{t}}}\right)\Bigg]\\ &\quad \times I(z)\sin\theta\cos\theta_{\mathrm{i}}\,\mathrm{d}\phi\,\mathrm{d}\theta, \quad (5)\end{aligned}$$

where $I(r_0,z_0,t)=I_0\mathrm{J}_0^2(k_{\mathrm{r}}r_0)$ is the intensity of the Bessel beam. θ_{i} is the angle of the incident light, θ_{t} is the angle of the reflected light, R and T are reflectance coefficient and transmittance coefficient, respectively.

The potential energy of a particle in a Bessel beam is related to the force and can be described as[20]

$$U(r,z)=-\int_0^r F_\rho(r_0,z_0)\,\mathrm{d}r_0. \quad (6)$$

Particle trapping is largely influenced by the environment. The particles can only be trapped when the potential barrier satisfies the condition, $\Delta U\geq 10k_{\mathrm{B}}T$,[31] in which k_{B} is the Boltzmann coefficient, and T is the temperature of the medium surrounding the particle.

3. Results and discussion

Beam profile and tunability are important parameters for multi-particle trapping and manipulation. And therefore, we first obtain dark–hollow beam (DHB) by using XPM in ethanol. The generated DHB further turns converged after an objective lens, and the Bessel beam can be obtained in the focusing region as shown in Fig. 3(a). It is seen that the DHB gradually involves into a beam with a bright central spot surrounded by a series of bright rings. It is also found that the lateral intensity distribution of the beam at focus is well fitted by the J_0 function, indicating that the beam is a good approximation of the Bessel beam (Fig. 3(b)). Moreover, as seen from the axial beam profile in the ρ–z plane in Fig. 3(a), the intensity of the Bessel beam keeps almost invariable in the focusing range, and non-diffraction range is ~ 0.04 mm. In addition, the number of the rings and the size of the central spot/rings are dependent on the pump power (Fig. 3(c)). We collect the

information about the number and size (the first ring is taken as an example) of the rings and plot them with respect to the pump power as shown in Fig. 3(d). It is observed that the size of the J_0 Bessel beam decreases almost linearly with respect to the pump power. And the number of rings increases with the pump power increasing.

The conversion of a Gaussian beam into a hollow beam can be theoretically treated by XPM and thermal nonlinear optical effect, which has been described in detail previously.[32–34] In brief, the strong Gaussian beam (pump beam, with intensity I_1) passes through the nonlinear medium (ethanol in this work) and the refractive index n of the ethanol becomes laser intensity-dependent ($n = n_0 + n_2 I_1$) due to thermal nonlinear effect. The distribution of the refractive index is applied to any beam that passes through the ethanol in the same area with the pump beam. Therefore, when the probe beam passes through the ethanol, an additional lateral phase shift $\Delta\varphi(r) = k_0 \int_0^l n_2 I_1 \, \mathrm{d}z$ on the exit plane of nonlinear medium is generated (k_0 is the wave vector). The probe beam carrying the nonlinear phase shift propagates in free space and forms a hollow beam as shown in the inset of Fig. 1(a). As the nonlinear phase shift $\Delta\varphi(r)$ is proportional to the intensity of the pump beam, the size of the hollow beam can be modulated by the power of the pump beam. With focusing through objective lens 1, the generated hollow beam becomes converged and converted into J_0 Bessel beam in the focusing range. In addition, the size of J_0 Bessel beam is dependent on the dark diameter of hollow beam at the given objective.[35] Therefore, the size of the J_0 Bessel beam can be modulated by the power of the pump beam.

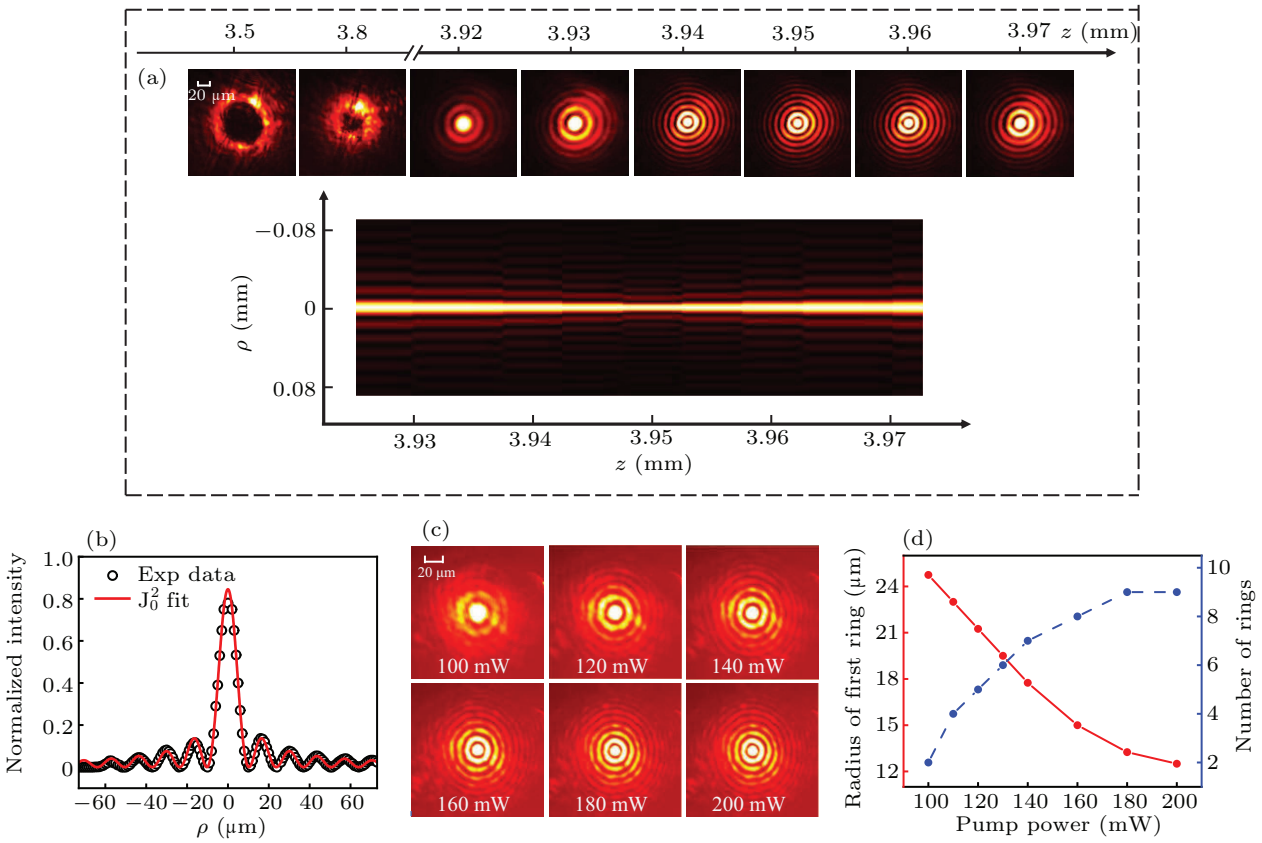


Fig. 3. Characteristics of beam profile and tunability in size of the J_0 Bessel beams. (a) Axial evolution of Bessel beam near the focal point, and axial beam profile in ρ–z plane, (b) lateral intensity distribution of beam and zero-order Bessel function fitting, and (c) images of beam as pump power varies from 100 mW to 200 mW, and (d) radius of the first ring (red solid) and number of rings (blue dashed) with respect to the pump beam power.

The obtained J_0 Bessel beam is used to trap the PS particles. The Bessel beam power is kept constant at ~ 65 mW, and the number concentration of PS particle suspension is $\sim 2 \times 10^6$ mL^{-1}. Experimentally, we find that the PS particles are driven towards the central bright spot once the laser is applied to the sample, and finally trapped in the central bright spot area and bright rings' area. Typical image of the trapped particles is shown in the insert of Fig. 4(a). It is seen that there are multiple particles trapped simultaneously. We also examine the stability of the trapped PS particles by tracking each particle in 2 minutes. For a given particle, its initial trapping position is taken as the origin (0). And then the distance from its position at a given time is noted down and plotted with respect to time, as shown in Fig. 4(b). Figure 4(c) further shows the projection of particle number on distance away from the origin, with the FHWM of the Gaussian fitting being ~ 0.7 μm.

We further calculate the force of trapping particles by using video tracking method.[36] We track the motion of a particle (the particle is denoted as a circle in video 1 in the sup-

porting information), noted down its position every 0.5 s and plot its trajectory of the particle moving towards to the central bright spot of the Bessel beam as shown in Fig. 4(d). With the help of the trajectory, we calculate the acceleration and further the trapping force as a function of position as shown by the points in Fig. 4(e).

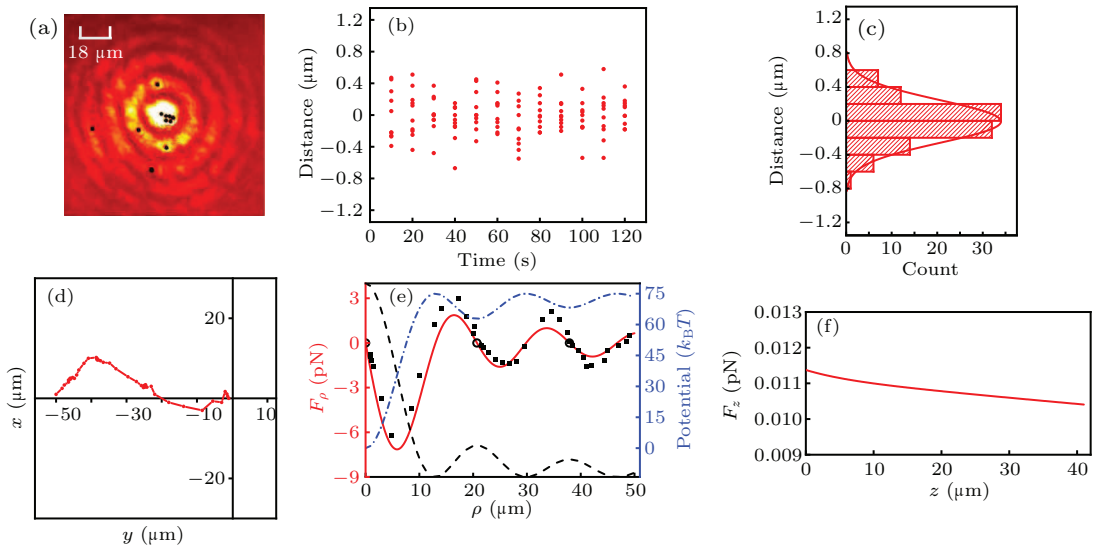


Fig. 4. (a) Typical image of trapped particles in Bessel beam. (b) Time-dependent positions of the trapped particles. (c) Projection of particle number on distance and the Gaussian fitting. (d) Trajectory of particle moving towards the central bright spot (origin of the coordinates). (e) Experimental data calculated trapping force of particle during movement (black squares), simulated optical radial force (red solid), and corresponding potential profiles (blue dash-dotted), and radial intensity distribution of J_0 Bessel beam (black dashed), with circles denoting traps. (f) Optical axial force in the Bessel beam along z axis.

To understand the mechanism that how particles are trapped in the central bright spot and the bright rings, we conduct the theoretical simulation and plot the force and potential that the particles experience in the J_0 Bessel beam as shown in Fig. 4(d). It is seen that the experimental results accord well with the overall distribution of the simulated results. It is seen that the experimental results are consistent with the overall distribution of the simulated results. But the comparison indicates that experimental force is higher than the theoretical one especially at the inner rings, which may be due to the fact that the scattering force also has a contribution to the particle movement. The scattering force is along the laser propagating direction, we call it axial optical force here. Figure 4(f) shows the axial optical force F_z exerted on the particle as a function of z. It is seen that F_z keeps almost constant along the z direction, which is to be expected for the non-diffraction property of the Bessel beam. And hence, there is a poor confinement of the particle along the laser propagating direction.

Owing to the spatially periodic optical field of the Bessel beam in the transverse direction, there are multiple optical potential wells, and the stable trapped position corresponds to the lowest potentials.[31] It is seen from the force curve in Fig. 4(d) that $F_\rho(r) = 0$ and the slope of the force curve is negative at the stable trapped positions, which means that there is a restoring force exerted on the particle in the opposite direction for any displacement of the particle, and therefore the particles can be confined around those points. In addition, the potential barrier is higher at the traps closer to the center of Bessel beam, and therefore there are more particles that are trapped in the center of the J_0 Bessel beam.

A lot of researches have demonstrated that there are particles hopping between the different side lobes in the laser trap using Bessel beam.[20,37] And this phenomenon can be explained by Eqs. (4) and (6). The radial force and the potential energy are influenced by the particle size and intensity distribution of trapped laser beam. When the particles size is bigger than ring width of Bessel beam, the particles will hop between different side lobes of Bessel beam.[37] The larger the numerical aperture of the objective lens, the smaller the size of the Bessel beam that can be generated and the smaller particles that can be trapped (as shown in Fig. S1 in supporting information). In the above mentioned work, the diameter of central bright spot and the first bright ring of Bessel beam are 22 μm and 12 μm respectively, which are much bigger than the particles size (3 μm). And therefore, once the particles are captured, hopping is not easy to occur.

In order to further elucidate the mechanism of the hopping between adjacent rings of Bessel beam, we use PS particles each with the diameter of 10 μm to study their motion between the rings of Bessel beams with various widths. When the width of central bright spot and the first bright ring of Bessel beam are 19.8 μm and 9.5 μm, respectively, we observe that the particles pass through the bright rings, and finally are trapped at the central bright spot as shown in Fig. 5(a). This can be explained by the simulation results as shown in Fig. 5(b), from which we can see the potential barriers at the

rings are rather low and therefore not enough to trap the particles. Then, when we increase the width of central bright spot and the first bright ring to 38 μm and 16 μm, the particle can be captured at either the central bright spot and the bright ring as shown in Fig. 5(c), which is due to deeper potential barrier shown in Fig. 5(d).

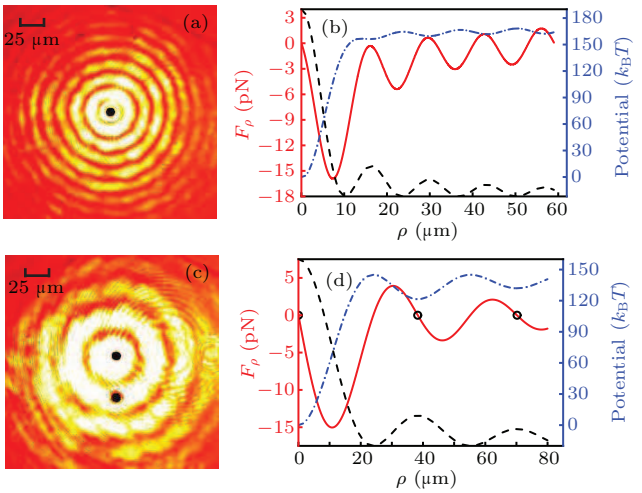


Fig. 5. The 10-μm-diameter particles trapped by Bessel beams with various sizes. (a) Typical image of particles trapped in Bessel beam with the width of central spot and first bright ring of 19.8 μm and 9.5 μm respectively. (b) Simulated optical radial force (red solid) and potential profiles (blue dash-dotted), and radial intensity distribution of J_0 Bessel beam (black dashed) related to the Bessel beam in panel (a) with circle denoting trap. (c) Typical image of trapped particles in Bessel beam with a width of central spot and first bright ring of 38 μm and 16 μm respectively. (d) Simulated optical radial force (red solid) and potential profiles (blue dash-dotted), and radial intensity distribution of J_0 Bessel beam (black dashed) related to the Bessel beam in panel (c) with circles denoting traps.

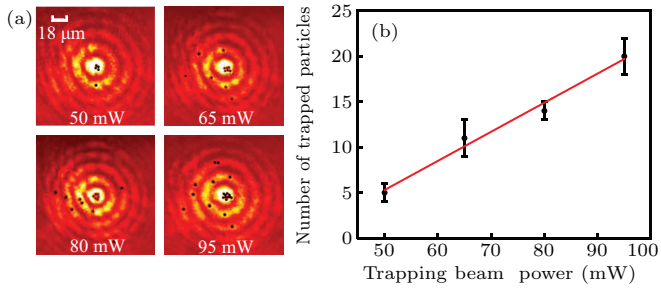


Fig. 6. Variations of trapped particle number with respect to the trapping beam power. (a) Images of trapped particles at trapping beam power 50 mW, 65 mW, 80 mW, and 95 mW. (b) Trapped particle number *versus* trapping beam power.

It is found that there are more particles trapped when the trapping laser power increases. Figure 6(a) shows the images of trapped particles under various power values of trapping laser beam. We can see that the particles are mainly trapped in the center of J_0 Bessel beam when the power of the trapping beams is $\sim$ 50 mW. As the trapping beam power increases, more and more particles are trapped at the bright rings. It is to be expected because the bright rings are strong enough to trap the particles when we increase the overall power. We further plot the number of trapped particles with respect to the power as shown in Fig. 6(b). It is seen that the total number of particles trapped increases almost linearly with the increasing trapping beam power.

The trapped particles (3 μm in diameter) can be transversely manipulated by modulating the size and number of rings of the J_0 Bessel beam. Experimentally, we keep the power of the trapping J_0 Bessel beam fixed at 100 mW and continuously increase the pump beam power from 135 mW to 185 mW. It is found that the trapped particles at the rings move transversely with radius of the rings varying according to the pump beam (Fig. 3) as shown in Fig. 7(a). To clearly demonstrate the results, we set the center of the J_0 Bessel beam to be origin and mark the lateral positions of trapped particles under various values of pump beam power. It is seen that the trapped particles move to the origin by a distance of $\sim$ 8 μm with the pump beam power increasing.

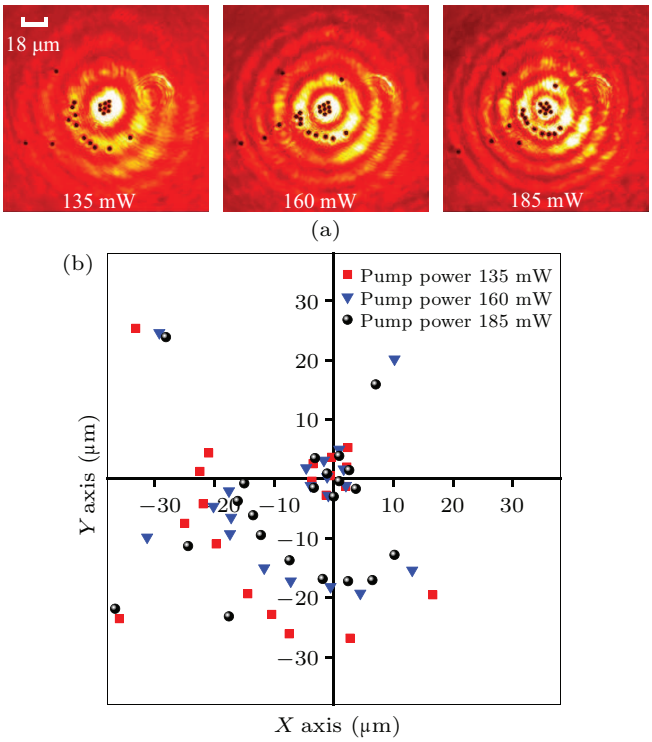


Fig. 7. Transverse manipulation of trapped particles with respect to pump beam power. (a) Images of trapped particles atr pump power of 135 mW, 160 mW, and 185 mW. (b) Positions of trapped particles at different pump beam power values.

4. Conclusions

In this work, we trapped and manipulated the particles transversely by size tunable J_0 Bessel beam obtained from XPM based on the thermal nonlinear optical effect. The results demonstrate that multiple PS particles can be stably trapped for two minutes in the liquid, and the number of the trapped PS particles can be controlled by trapped power. In addition, the trapped PS particles can be manipulated laterally with a micron-level precision by changing the size of J_0 Bessel beam. Compared with other devices that produce multiple optical traps, our setup is flexible, low-cost, and easy to use. Moreover, this particle manipulation method of changing the size of

the Bessel beam is superior to other methods. The merits of high trapping efficiency and simple operation give this method a great potential for the *in-situ* study of multiple particles and a convenient tool in many areas, such as cell sorting and transportation.

Acknowledgements

Project supported by the National Natural Science Foundation of China (Grant Nos. 61805200, 51927804, and 12104365), the Natural Science Foundation of Shaanxi Province, China (Grant No. 2020JM-432), the Fund for Young Star in Science and Technology of Shaanxi Province, China (Grant No. 2021KJXX-27), and the Fund from the Education Department of Shaanxi Province, China (Grant No. 21JK0915).

References

[1] Ashkin A, Dziedzic J M, Bjorkholm J E and Chu S 1986 *Opt. Lett.* **11** 288
[2] Ashkin A, Dziedzic J M and Yamane T 1987 *Nature* **330** 769
[3] Ojeda J F, Xie C, Li Y Q, Bertrand F E, Wiley J and McConnell T J 2006 *Opt. Express* **14** 5385
[4] Zhu C L and Li J 2015 *Chin. Phys. Lett.* **32** 108702
[5] Miles R E, Walker J S, Burnham D R and Reid J P 2012 *Phys. Chem. Chem. Phys.* **14** 3037
[6] Yang Y, Zhang G and Dai X 2020 *Chin. Phys. B* **29** 057302
[7] O'Neil A T, MacVicar I, Allen L and Padgett M J 2002 *Phys. Rev. Lett.* **88** 053601
[8] Huisken J and Stelzer E H K 2002 *Opt. Lett.* **27** 1223
[9] Gong Z, Pan Y L, Videen G and Wang C 2018 *J. Quant. Spectrosc. Ra.* **214** 94
[10] Tanaka Y 2013 *J. Optics-uk* **15** 025708
[11] Tanaka Y and Wakida S 2015 *Biomed. Opt. Express* **6** 3670
[12] Habaza M, Gilboa B, Roichman Y and Shaked N T 2015 *Opt. Lett.* **40** 1881
[13] Shaw L A, Panas R M, Spadaccini C M and Hopkins J B 2017 *Opt. Lett.* **42** 2862
[14] Chiou A E, Wang W, Sonek G J, Hong J and Berns M W 1997 *Opt. Commun.* **133** 7
[15] Mohammadnezhad M, Saeed S R and Hassanzadeh A 2019 *J. Optics-uk* **21** 105404
[16] Durnin J, Miceli J J and Eberly J H 1987 *Phys. Rev. Lett.* **58** 1499
[17] Xie Y, Lei T, Yang C, Du L and Yuan X 2019 *Chin. Opt. Lett.* **17** 090602
[18] Arlt J, Garcés-Chávez V, Sibbett W and Dholakia K 2001 *Opt. Commun.* **197** 239
[19] Garcés-Chávez V, McGloin D, Melville H, Sibbett W and Dholakia K 2002 *Nature* **419** 145
[20] Milne G, Dholakia K, McGloin D, Volke-Sepulveda K and Zemánek P 2007 *Opt. Express* **15** 13972
[21] Volke-Sepúlveda K, Chávez-Cerda S, Garcés-Chávez V and Dholakia K 2004 *Josa. B* **21** 1749
[22] Garcés-Chávez V, Volke-Sepulveda K, Chávez-Cerda S, Sibbett W and Dholakia K 2002 *Phys. Rev. A* **66** 063402
[23] Scott G and McArdle N 1992 *Opt. Eng.* **31** 2640
[24] Ayala Y A, Arzola A V and Volke-Sepulveda K 2016 *Opt. Lett.* **41** 614
[25] Zhang Q, Cheng X M, Chen H W, He B, Ren Z Y, Zhang Y and Bai J T 2017 *Appl. Phys. Lett.* **111** 161103
[26] Cheng X M, Zhang Q, Chen H W, He B, Ren Z Y, Zhang Y and Bai J T 2017 *Opt. Express* **25** 25257
[27] Ashkin A 1992 *Biophys. J.* **61** 569
[28] Wright W H, Sonek G J and Berns M W 1993 *Appl. Phys. Lett.* **63** 715
[29] Ambrosio L A and Hernández-Figueroa H E 2009 *Opt. Express* **17** 21918
[30] Gussgard R, Lindmo T and Brevik I 1992 *Josa. B.* **9** 1922
[31] Harada Y and Asakura T 1996 *Opt. Commun.* **124** 529
[32] He B, Cheng X M, Zhang H, Chen H W, Zhang Q, Ren Z Y and Bai J T 2018 *Appl. Phys. Express* **11** 052501
[33] Castaldo F, Paparo D and Santamato E 1997 *Opt. Commun.* **143** 57
[34] Zhang Q, Cheng X M, He B, Chen H W, Ren Z Y and Bai J T 2019 *Opt. Laser Technol.* **119** 105582
[35] Tiwari S K, Mishra S R, Ram S P and Rawat H S 2012 *Appl. Opt.* **51** 3718
[36] Rohrbach A, Tischer C, Neumayer D, Florin E L and Stelzer E H 2004 *Rev. Sci. Instrum.* **75** 2197
[37] Bobkova V, Stegemann J, Droop R, Otte E and Denz C 2021 *Opt. Express* **29** 12967